2260–2270 *Nucleic Acids Research, 2011, Vol. 39, No. 6* *Published online 9 November 2010*
doi:10.1093/nar/gkq1127

eIF4G stimulates the activity of the DEAD box protein eIF4A by a conformational guidance mechanism

Manuel Hilbert, Fabian Kebbel, Airat Gubaev and Dagmar Klostermeier*

University of Basel, Biozentrum, Dept. of Biophysical Chemistry, Klingelbergstrasse 70, CH–4056 Basel, Switzerland

Received June 30, 2010; Accepted September 11, 2010

ABSTRACT

The activity of eIF4A, a key player in translation initiation, is regulated by other translation factors through currently unknown mechanisms. Here, we provide the necessary framework to understand the mechanism of eIF4A's regulation by eIF4G. In solution, eIF4A adopts a defined conformation that is different from the crystal structure. Binding of eIF4G induces a 'half-open' conformation by interactions with both domains, such that the helicase motifs are pre-aligned for activation. A primary interface acts as an anchor for complex formation. We show here that formation of the secondary interface is essential for imposing the 'half-open' conformation on eIF4A, and it is critical for the functional interaction of eIF4G with eIF4A. Via this bipartite interaction, eIF4G guides the transition of eIF4A between the 'half-open' and closed conformations, and stimulates its activity by accelerating the rate-limiting step of phosphate release. Subtle changes induced by eIF4G may be amplified by input signals from other translation factors, leading to an efficient regulation of translation initiation.

INTRODUCTION

Translation initiation is a complex, multi-step process that is mediated by the combined action of a large number of translation initiation factors (1). As the rate-limiting step during protein synthesis, it is subject to tight regulation (2). The eukaryotic translation initiation factor 4A (eIF4A) is a unique component of the translation initiation factor network. As a member of the DEAD box protein family, it is an RNA-dependent ATPase, and consists of two flexibly linked RecA domains that carry a set of conserved motifs involved in ATP binding and hydrolysis, RNA binding and coupling of these activities (3). eIF4A shows only weak helicase activity (4,5) that is stimulated by the translation initiation factors eIF4B (or its homolog eIF4H), eIF4E and eIF4G (6–8). eIF4G functions as a scaffold protein that mediates interactions between eIF4A and other translation factors (1,2). eIF4A is thought to unwind secondary structures in the 5′-untranslated region of mRNAs to facilitate scanning of the 40S ribosomal subunit towards the start codon (9).

As a prototypic member of the DEAD box protein family (5), eIF4A has been studied intensively (10–13), and the first DEAD box protein structures determined were domains of eIF4A (14–16), and the complete eIF4A (16). The two RecA domains in eIF4A are arranged into a dumbbell-like shape, lacking any interdomain contacts. Structures of a number of DEAD box proteins have revealed that the juxtaposition of the two RecA domains in the absence of ligands varies between different DEAD box proteins, but they share as a common feature two RecA domains separated by a cleft that is lined by conserved motifs. By contrast, DEAD box proteins in complex with ligands adopt a compact structure with extensive contacts between the two RecA domains, and between conserved motifs of both RecA domains and the bound nucleotide and RNA (17–22). According to the current model for DEAD box protein activity [reviewed in ref. (3), see also references therein], cooperative binding of ATP and RNA triggers the formation of the closed conformer (10,11,23), leading to the assembly of the catalytic site for ATP hydrolysis and of the bipartite RNA binding site formed by both RecA domains (17). After ATP hydrolysis, presumably upon phosphate release (24), the cleft between the two RecA domains reopens, leading to a release of the bound RNA, and resetting the enzyme for further catalytic cycles (25). The transition between open and closed conformations is intimately linked to DEAD box protein function, and a regulation via affecting this

*To whom correspondence should be addressed. Tel: +41 61 267 2381; Fax: +41 61 267 2189; Email: dagmar.klostermeier@unibas.ch

© The Author(s) 2010. Published by Oxford University Press.
This is an Open Access article distributed under the terms of the Creative Commons Attribution Non-Commercial License (http://creativecommons.org/licenses/by-nc/2.5), which permits unrestricted non-commercial use, distribution, and reproduction in any medium, provided the original work is properly cited.

Downloaded from https://academic.oup.com/nar/article-abstract/39/6/2260/2411439/eIF4G-stimulates-the-activity-of-the-DEAD-box
by WWZ Bibliothek (Oeffentliche Bibliotherk der UniversitÃ¤t Basel) user
on 10 October 2017

conformational change is conceivable. The stimulation of eIF4A activity by eIF4G has been addressed in previous studies. A 'soft clamp' model for the stimulation of eIF4A activity by eIF4G has been put forward, in which eIF4G contacts both RecA domains of eIF4A simultaneously, and thereby restricts eIF4A in the closed conformation (26). An extended study that addressed the topology of the eIF4A/eIF4G/eIF4H complex suggested that a network of specific, highly dynamic interactions of eIF4G and eIF4H with eIF4A regulates its conformational cycle (27). The recently reported crystal structure of yeast eIF4A in complex with the eIF4A-binding domain of eIF4G confirmed the two interaction sites (28): A primary interface is formed by the C-terminal RecA domain of eIF4A and the N-terminal region of eIF4G, and a secondary interface is formed by the N-terminal RecA domain and the C-terminal part of eIF4G (Figure 1A). In the complex, no contacts between the two RecA domains of eIF4A are formed, but the two RecA domains are much closer than in the earlier reported crystal structure of the open conformation (16). The authors conclude that the secondary interface between eIF4A and eIF4G will be disrupted upon formation of the closed eIF4A conformer, and suggest that eIF4G acts as a 'stopper' that prevents the N-terminal domain of eIF4A from moving too far away (28).

Here, we investigate the interaction between yeast eIF4A and the eIF4A-binding domain of eIF4G. In single molecule Förster resonance energy transfer (smFRET) experiments, we map the conformation of eIF4A in solution and show that it is different from the crystal structure. Furthermore, we correlate the conformational change that eIF4G induces in eIF4A with the formation of the secondary interface, and with eIF4G's stimulation of the eIF4A ATPase activity. The eIF4G-stabilized conformation of eIF4A is distinct from the open and closed conformations. In this 'half-open' conformation, nucleotide exchange and phosphate release are facilitated. We propose a conformational guidance model for eIF4G-stimulated activity of eIF4A, in which the N-terminal domain of eIF4A alternates between interactions with eIF4G in the 'half-open' conformation, and with the C-terminal domain of eIF4A in the closed conformation, allowing for accelerated progression through the catalytic cycle.

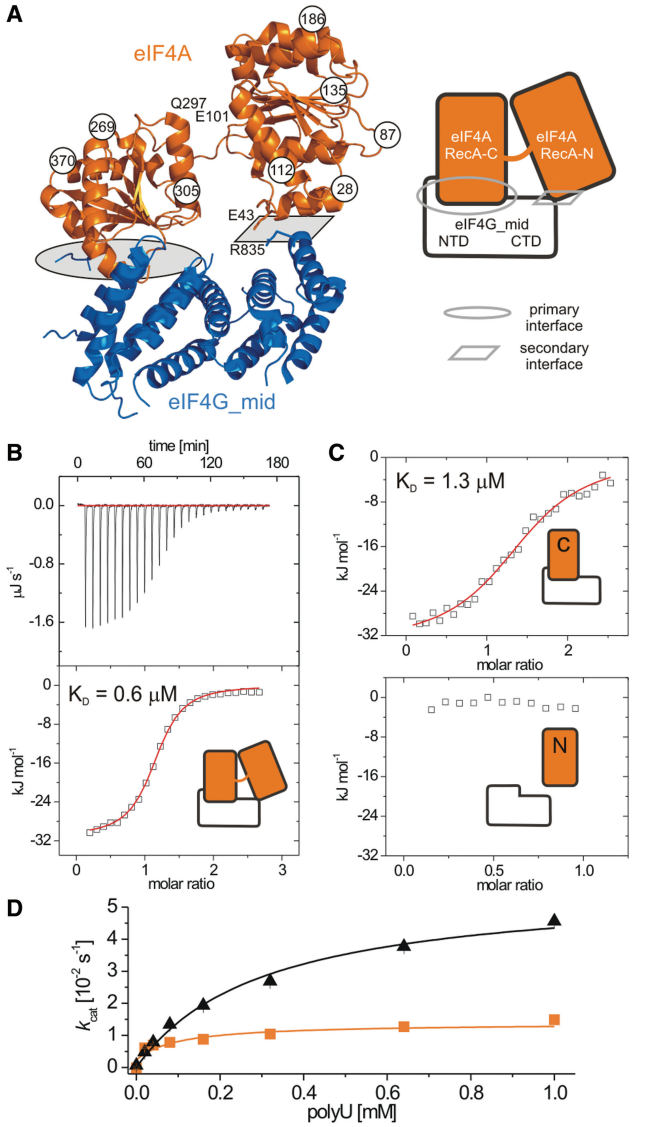

Figure 1. Interaction between eIF4A and eIF4G and contributions of the eIF4A RecA domains to complex formation. (**A**) Architecture of eIF4A/eIF4G_mid complex (PDB-ID 2vso) (28). eIF4A is depicted in orange, eIF4G in blue. The primary interface, formed by the C-terminal domain of eIF4A and the N-terminal part of eIF4G, and the secondary interface are marked. Important residues studied in this work (E43, E101 and Q297 in eIF4A, R835 in eIF4G) are highlighted. Residues indicated by circled numbers denote positions for fluorophore attachment. The pictogram represents the simplified representation of the eIF4A/eIF4G complex used throughout all figures. (**B**) Isothermal calorimetric titration of eIF4A with eIF4G. The K_d value of the eIF4A/eIF4G complex is $0.6 \pm 0.1\,\mu M$. (**C**) ITC titration of the isolated N- and C-terminal domains of eIF4A with eIF4G. The dissociation constant for the RecA_C/eIF4G complex is $1.3 \pm 0.1\,\mu M$. No binding is detected for RecA_N, indicating that the secondary interface does not contribute significantly to complex stability. (**D**) Steady-state ATPase activity of eIF4A in the absence (orange squares) and presence (black triangles) of eIF4G. eIF4G stimulates the intrinsic ATPase activity of eIF4A ~5-fold. The k_{cat} values are $k_{cat} = 0.012 \pm 0.002\,s^{-1}$ (–eIF4G) and $k_{cat,stim} = 0.057 \pm 0.003\,s^{-1}$ (+eIF4G).

MATERIAL AND METHODS

Site-directed mutagenesis, protein production and purification

Plasmids encoding the genes for eIF4A and eIF4G_mid (aa 572–853) were provided by Ulrich Baumann (University of Bern). Site-directed mutagenesis was performed according to the Quikchange protocol (Stratagene). eIF4A-RecA_N (aa 1–224) was constructed by introducing a stop codon after the codon for aa 224. For eIF4A-RecA_C (aa 226-406), an NdeI restriction site was introduced after the coding region for aa 1–225, and the region between the two NdeI restriction sites was deleted by cleavage and subsequent religation. Correct sequences were confirmed for all constructs. eIF4G_mid contains the conservative mutation K590R. All experiments described in this manuscript have been performed with eIF4G_mid.

Downloaded from https://academic.oup.com/nar/article-abstract/39/6/2260/2411439/eIF4G-stimulates-the-activity-of-the-DEAD-box
by WWZ Bibliothek (Oeffentliche Bibliotherk der UniversitÃ¤t Basel) user
on 10 October 2017

Proteins were produced and purified after Schütz *et al.* (28) with minor modifications. Both proteins were produced in auto-inducing medium (29) during 24 h. eIF4A was produced in *Escherichia coli* BL21(DE3) at 37°C, and eIF4G_mid in *E. coli* BL21(DE3) CodonPlus RP (Stratagene) at room temperature.

Cells were disrupted in a microfluidizer in 50 mM Tris/HCl, pH 7.5, 1 M NaCl and 2 mM β-mercaptoethanol (BME) in the presence of protease inhibitors (Roche). Cell debris was separated by centrifugation. The supernatant was supplemented with 10 mM imidazole and applied to a Ni^{2+}–NTA column (GE Healthcare) equilibrated in 50 mM Tris/HCl, pH 7.5, 500 mM NaCl, 10 mM imidazole and 2 mM BME at 4°C. The proteins were eluted with the same buffer with 500 mM imidazole. The hexahistidine-tag was cleaved with thrombin (GE Healthcare) during overnight dialysis against imidazole-free buffer. Uncleaved protein was removed via a second Ni^{2+}–NTA column. The flow through was concentrated and purified on a size-exclusion S75 column (GE Healthcare) equilibrated in 50 mM Tris/HCl, pH 7.5, 200 mM NaCl, 2 mM BME. Protein containing fractions were pooled, concentrated, shock-frozen in liquid nitrogen and stored at −80°C. Protein purity was >95% as judged from Coomassie stained sodium dodecyl sulfate polyacrylamide gels. Concentrations were determined photometrically using the extinction coefficients $\varepsilon = 18\,005\,M^{-1}\,cm^{-1}$ (eIF4A) and $\varepsilon = 35\,200\ M^{-1}\,cm^{-1}$ (eIF4G_mid), calculated with ProtParam (30).

Fluorescence equilibrium titrations

Nucleotides were purchased from Jena Biosciences. Dissociation constants of eIF4A/nucleotide complexes at 25°C were determined in fluorescence equilibrium titrations in a Jobin Yvon FluoroMax3 fluorimeter with the fluorescent mantADP (31). Mant fluorescence was excited at 360 nm (2 nm bandwidth) and detected at 440 nm (2 nm bandwidth). 1 μM mantADP in buffer A (50 mM Tris/HCl, pH 7.5, 80 mM KCl, 2.5 mM $MgCl_2$, 1 mM dithiothreitol, 1% glycerol) was titrated with eIF4A up to 60 μM. The nucleotide affinity of the eIF4A/eIF4G_mid complex was determined in presence of 100 μM eIF4G_mid to ensure saturation. The K_d value was determined using the solution of the quadratic equation describing a 1:1 complex formation [Equation (1)]:

$$F = F_0 + \frac{\Delta F_{max}}{[L]_{tot}} \cdot \left(\frac{[E]_{tot} + [L]_{tot} + K_d}{2} - \sqrt{\left(\frac{[E]_{tot} + [L]_{tot} + K_d}{2} \right)^2 - [E]_{tot}[L]_{tot}} \right) \quad (1)$$

F_0 is the fluorescence of free mantADP, ΔF_{max} is the amplitude, $[E]_{tot}$ the total enzyme concentration and $[L]_{tot}$ the total ligand concentration.

The dissociation constants of eIF4A/adenine nucleotide complexes were determined in competitive titrations of the mantADP/protein complex with ADP and ADPNP. The solution of the cubic equation describing the competitive titration was evaluated numerically using the program Scientist (Micromath) to yield the K_d of the respective nucleotide complex.

Steady-state ATPase activity

The steady-state ATPase activity of eIF4A was measured in a coupled ATPase assay (32) in buffer A with 2 mM ATP, 0.4 mM phosphoenol pyruvate, 0.2 mM NADH, 13 μg ml^{-1} lactate dehydrogenase and 23 μg ml^{-1} pyruvate kinase at 37°C via the decrease in A_{340} due to oxidation of NADH to NAD^+. The concentrations were 1 μM (eIF4A) and 6 μM (eIF4G). polyU-RNA (GE Healthcare), a frequently used model substrate for DEAD box helicases with little or no substrate specificity, was used as an RNA substrate for eIF4A. polyU-RNA concentrations were varied from 0 to 1 mM (bases) to determine $K_{M,RNA}$ values. Initial velocities v (in μM ATP s^{-1}) were calculated from the absorbance change $\Delta A_{340}/\Delta t$ with $\varepsilon_{340,\ NADH} = 6\,300\,M^{-1}\,cm^{-1}$, and converted to k_{cat}. Data were analyzed according to the Michaelis–Menten equation.

Phosphate release

The release of phosphate was detected by an MDCC-PiBiP (phosphate-binding-protein) phosphate sensor (0.5 μM, Invitrogen) in buffer A at 37°C in the presence of 2 μM eIF4A, 6 μM eIF4G_mid, 2 mM ATP and 1 mM polyU-RNA. Free phosphate was removed by the addition of phosphate mop (0.01 U/ml PNPase and 200 μM 7-methyl guanosine, Sigma) (33) to the cuvette and the ATP stock solution. The reaction was started by addition of ATP. MDCC-PiBiP fluorescence was monitored at 485 nm in a Jobin Yvon FluoroMax3 fluorimeter (excitation: 425 nm, excitation/emission bandwidth 1 nm and 2 nm). Due to the low MDCC-PiBiP concentrations, the observed time trace describes single turnover phosphate release. Rates of phosphate release were determined from a single exponential fit.

Isothermal titration calorimetry

Isothermal titration calorimetry experiments were conducted on a VP-ITC (MicroCal). Binding of eIF4A and eIF4G_mid was measured in 50 mM Tris/HCl, pH 7.5, 80 mM KCl at 15°C. The proteins in the cell (20–30 μM) and syringe (200–300 μM) were transferred into identical buffers with NAP-5 columns (GE Healthcare). In all titrations shown, eIF4A was added to eIF4G, but reverse titrations delivered similar results. For the determination of nucleotide affinity, the buffer contained 15 mM $MgCl_2$. Nucleotides were directly dissolved in buffer, and the pH was adjusted with KOH. The nucleotide concentration in the syringe was 2–4 mM. Titrations were performed in 10 μl steps at a stirring speed of 305 s^{-1} and a reference power of 71 μJ s^{-1} (17 μcal s^{-1}). The data were integrated with Origin for MicroCal ITC and analyzed with a one-site binding model.

smFRET experiments

Proteins were labeled with a mixture of A488- (donor) and A546-maleimide (acceptor), respectively, for 1 h at 25°C

Downloaded from https://academic.oup.com/nar/article-abstract/39/6/2260/2411439/eIF4G-stimulates-the-activity-of-the-DEAD-box
by WWZ Bibliothek (Oeffentliche Bibliotherk der UniversitÃ¤t Basel) user
on 10 October 2017

in the presence of 1 mM Tris(2-carboxyethyl)phosphine. The ratio of the dyes was varied around 1:4:8 (protein:donor:acceptor) to maximize the yield of donor/acceptor-labeled protein. Labeling efficiencies were determined from absorbance ratios at 495 nm (A488, corrected for A546 contributions) or 555 nm (A546) and 280 nm (protein, corrected for dye contributions). SmFRET experiments were performed in a home-built confocal microscope as described (23). All measurements were performed at room temperature in buffer A treated with active charcoal with 50 pM fluorescently labeled eIF4A (concentration of donor fluorophore) and 10 μM of eIF4G_mid. Only fluorescence bursts above a threshold of 100 photons were considered in the analysis. Measured fluorescence intensities were corrected for background. For calculating FRET histograms, the raw intensities were corrected for crosstalk of donor fluorescence into the acceptor channel (α), for cross talk of acceptor fluorescence into the donor channel (β), for differences in quantum yields and detection efficiencies for donor and acceptor fluorescence (γ), and for direct excitation of the acceptor (δ) as described previously (23). Correction parameters and were determined individually for each construct as described (23), and are summarized in Supplementary Table 1. From experimental uncertainties in the determination of correction parameters, the experimental errors for FRET efficiencies are <5%.

The Förster distances R_0 were also determined individually for each construct (Supplementary Table 1) and used to convert FRET efficiencies of single molecules into inter-dye distances to create distance histograms. Distance histograms were described with a Gaussian distribution. This analysis yielded a mean inter-dye distance, determined with standard deviations <0.1 nm, and a width of the distribution, σ, that contains contributions from shot noise, from the local flexibility of the dyes due to flexible linkers and from the global flexibility of the protein. Importantly, differences in the mean distance for the same construct determined in independent experiments do not exceed 0.1 nm.

To further validate the calculated FRET efficiencies, they were independently determined from lifetimes of the donor in single molecules carrying a donor only, or a donor and an acceptor (Supplementary Figure 2).

Nucleotide binding kinetics

Nucleotide exchange kinetics were measured in an SX18 stopped flow fluorimeter (Applied Photophysics) in buffer A at 15°C. Pseudo-first-order conditions were ensured by an excess of mantADP over protein. Protein-bound mantADP was selectively detected by excitation via energy transfer from tryptophan. For this purpose, Y22W was introduced into eIF4A. mantADP bound to the eIF4A/eIF4G_mid complex was excited by energy transfer from intrinsic tryptophans in eIF4G_mid. Tryptophan fluorescence was excited at 280 nm, and the mant fluorescence was detected through a 400 nm cut-off long pass filter (Schott). At least four traces where recorded and averaged, and described with single (RecA_N) or double exponential functions. For eIF4A and eIF4A/eIF4G_mid, rate constants of individual steps, k_1, k_{-1}, k_2 and k_{-2}, were extracted from the dependence of the observed rate constants ($\lambda_{1,2}$) on the mantADP concentration [mA] with a two-step binding model (34) using Equation (2):

$$\lambda_{1,2} = \frac{(k_1[mA] + k_{-1} + k_2 + k_{-2}) \pm \sqrt{(k_1[mA] + k_{-1} + k_2 + k_{-2})^2 - 4(k_1[mA](k_2 + k_{-2}) + k_{-1}k_2)}}{2} \quad (2)$$

The rate of mantADP dissociation k_{off} was determined at 37°C by displacing mantADP from the protein complex in the presence or absence of polyU-RNA with 10 mM ADP with direct excitation of mantADP fluorescence at 355 nm.

RESULTS

Mapping the conformation of eIF4A in solution: eIF4G stabilizes a distinct, 'half-open' conformation of eIF4A

To provide a framework for dissecting the mechanism of eIF4G-stimulated eIF4A activity, we quantified the interaction eIF4A and a construct comprising aa 572–853 of eIF4G (Figure 1A; eIF4G_mid). This so-called 'middle domain' is sufficient for binding to eIF4A, and for stimulation of its ATPase activity (Figure 1B and D) (28). The K_d value of the eIF4A/eIF4G complex is 0.6 ± 0.1 μM (Figure 1B), and the rate constant for ATP hydrolysis by eIF4A is ~5-fold increased by eIF4G in the presence of polyU-RNA (Figure 1D).

In the crystal structure of the eIF4A/eIF4G complex, eIF4G contacts both RecA-like domains of eIF4A (28); (Figure 1A). The two RecA domains are closer than in the structure of unliganded eIF4A (16) (PDB-ID 1fuu), prompting the authors to suggest that eIF4G restricts the N-terminal domain from moving too far away. However, the crystal structure of eIF4A shows the largest separation of the two RecA domains among all DEAD box protein structures reported to date, and thus may not be a suitable reference. We therefore probed the conformation of eIF4A in solution in smFRET experiments with Alexa488- (A488-, donor) and Alexa546- (A546-, acceptor) labeled eIF4A. Constructs used were eIF4A_E28/G370C, eIF4A_S87/G370C, eIF4A_A112/G370C, eIF4A_E135/G370C, eIF4A_Q186/E269C, eIF4A_Q186/E305C and eIF4A_Q186/G370C (Figure 1A). All proteins showed wild-type-like circular dichroism spectra (Supplementary Figure 1), and RNA-stimulated ATPase activities that are similar to wild-type and are stimulated by eIF4G. In the absence of eIF4G, FRET efficiencies of 0.65 ± 0.02 (E28/G370C), 0.22 ± 0.02 (S87/G370C), 0.71 ± 0.01 (A112/G370C), 0.30 ± 0.01 (E135/G370C), 0.53 ± 0.01 (Q186/E269C), 0.41 ± 0.01 (Q186/E305C) and 0.45 ± 0.01 (Q186/G370C) were obtained from Gaussian fits of the corrected FRET histograms (Figure 2A, see 'Materials and Methods' section and Supplementary Table 1 for details of data correction). The unimodal distributions of FRET efficiencies demonstrate that eIF4A adopts a

Downloaded from https://academic.oup.com/nar/article-abstract/39/6/2260/2411439/eIF4G-stimulates-the-activity-of-the-DEAD-box
by WWZ Bibliothek (Oeffentliche Bibliotherk der UniversitÃ¤t Basel) user
on 10 October 2017

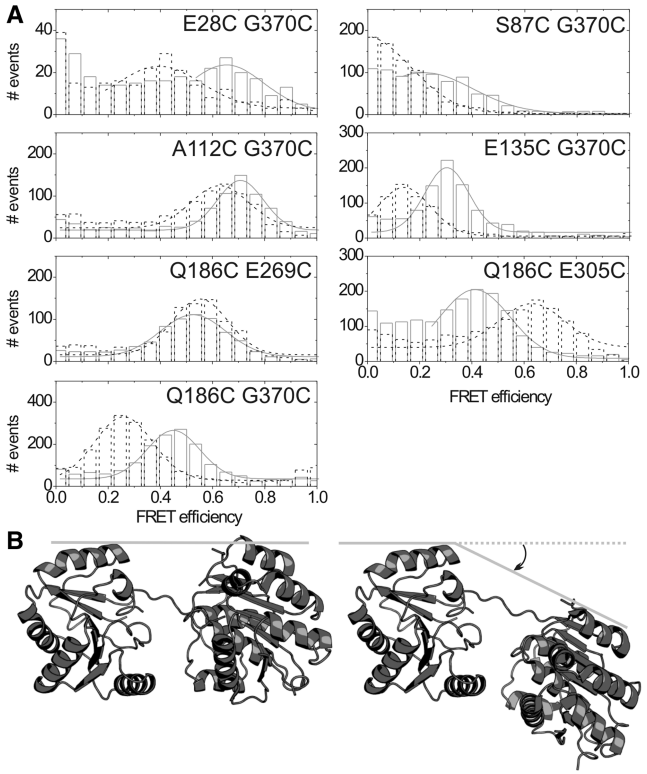

Figure 2. Conformation of eIF4A in absence and presence of eIF4G. (**A**) smFRET histograms for donor/acceptor-labeled eIF4A in the absence (solid line) and presence (broken line) of eIF4G. The positions for fluorophore attachment are indicated (see also Figure 1A). The FRET efficiencies decrease upon addition of eIF4G for eIF4A_E28/G370C, eIF4A_S87/G370C, eIF4A_E135/G370C and eIF4A_Q186/G370C, and increase for eIF4A_Q186/E305C. For eIF4A_A112/G370C and eIF4A_Q186/T269C, only minor changes are observed. (**B**) Reconstruction of the open conformation of eIF4A in solution (left) from changes in FRET efficiencies, and the eIF4G-stabilized conformation as captured in the crystal structure (PDB-ID 2vso, right). See main text for details. Compared to the crystal structure of eIF4A (PDB ID 1fuu), the separation of the two RecA domains in eIF4A is smaller in the conformation derived from smFRET measurements, and the conserved motifs are pointing more toward each other.

well-defined conformation in solution in the absence of binding partners. Our previous work has established that the corrected FRET efficiencies can be used to reliably calculate inter-dye distances. Inter-dye distances determined from smFRET experiments with donor/acceptor-labeled DNA were in very good agreement with values expected from B-form DNA geometry (35). Furthermore, for well-defined proteins of limited flexibility, we have previously reported inter-dye distances from FRET experiments that are in reasonable agreement with distances expected from their crystal structures (or structures of homologous proteins, refs. 23 and 35, Supplementary Figure 2). Therefore, we converted the FRET efficiencies of each individual eIF4A molecule into an inter-dye distance, and calculated distance histograms. The mean inter-dye distance was determined by describing the distance distributions in the distance histograms with a Gaussian distribution. The standard deviation for all mean distances was <0.1 nm (Table 1). In conjunction, the distances obtained define an open conformation of the helicase core in eIF4A (see below for construction of the open conformation of eIF4A in solution from FRET data).

When eIF4G was added to eIF4A (Figure 2A), the FRET efficiencies decreased for eIF4A_E28/G370C (0.40 ± 0.03), eIF4A_S87/G370C (0), eIF4A_E135/G370C (0.14 ± 0.01) and eIF4A_Q186/G370C (0.26 ± 0.01), and increased for eIF4A_Q186/E305C (0.63 ± 0.01). For eIF4A_A112/G370C (0.64 ± 0.01) and eIF4A_Q186/T269C (0.55 ± 0.01), the FRET efficiencies showed only minor changes. All experimental distances (Table 1) are comparable to the distances in the structure of the eIF4A/eIF4G complex [PDB-ID 2vso; (28)], confirming a similar conformation of the eIF4A/eIF4G complex in solution, and, at the same time, validating the extraction of reliable distance information from our single-molecule FRET experiments (Supplementary Figure 2).

Distance restraints from quantitative FRET experiments allow for mapping of global conformations. To reconstruct the conformation of eIF4A in solution, we calculated the differences of inter-dye distances in the eIF4A/eIF4G complex and in free eIF4A (Table 1).

Table 1. Comparison of experimental distances in solution with crystal structures

	eIF4A (smFRET)		eIF4A (1fuu)	eIF4A/eIF4G (smFRET)		eIF4A/eIF4G (2vso)
	r (nm)	σ (nm)	r (nm)	r (nm)	σ (nm)	r (nm)
E28/G370C	5.6 ± 0.09	0.85	6.4	5.8 ± 0.05	0.65	5.9
S87/G370C	6.7 ± 0.07	0.98	7.3	>7	1.22	7.1
A112/G370C	4.7 ± 0.02	0.43	5.9	4.8 ± 0.03	0.48	5.1
E135/G370C	6.6 ± 0.02	0.45	6.9	7.3 ± 0.04	0.80	6.6
Q186/E269C	5.4 ± 0.02	0.49	5.7	5.2 ± 0.02	0.41	4.9
Q186/E305C	6.4 ± 0.05	0.61	6.1	5.2 ± 0.04	0.64	4.1
Q186/G370C	6.3 ± 0.02	0.48	5.3	6.8 ± 0.02	0.64	6.1

Distances are means of distance histograms calculated from smFRET data, or C_β-C_β-distances measured from the crystal structures, respectively. In case of G370, the C_α was used for distance measurements from the crystal structure.
E135 was not included in the structural model, hence the distance given for E135/G370C is the distance from the C_α of G136 to the C_α of G370.
σ denotes the width of the Gaussian describing the distance distribution, and contains contributions from the local flexibility of the attached dyes, and the global flexibility of eIF4A.

Downloaded from https://academic.oup.com/nar/article-abstract/39/6/2260/2411439/eIF4G-stimulates-the-activity-of-the-DEAD-box
by WWZ Bibliothek (Oeffentliche Bibliotherk der UniversitÃ¤t Basel) user
on 10 October 2017

The same differences of inter-dye distances are obtained when FRET efficiencies are calculated from donor lifetimes for individual molecules (Supplementary Figure 2). In comparison to modeling the eIF4A conformation directly from the inter-dye distances, a reconstruction using changes in distances should minimize contributions from the length of the linker between the fluorophores and the cysteines. Starting from the conformation of eIF4A in complex with eIF4G as captured in the crystal structure (28), the position of the C-terminal RecA domain that forms the primary interface with eIF4G was kept in a fixed orientation, and the N-terminal domain was manually positioned according to the changes in distance derived from the smFRET experiments (Figure 2B). In the resulting model, eIF4A is in an open conformation. However, the two domains are significantly rotated, and the separation of the RecA domains is smaller than in the crystal structure (PDB-ID 1fuu).

From the comparison of the two conformations, it becomes evident that eIF4G re-orients the two RecA-like domains of eIF4A, but to a much smaller extent than previously thought. A rotation of the N-terminal RecA domain brings the conserved motifs closer together, and orients them toward each other. As a result, the inter-domain cleft is almost closed at the distal end from the eIF4G binding site, but remains open at the proximal end. The conformation stabilized by eIF4G is thus distinct from the open conformation we defined here for the first time, and from the closed conformation of eIF4A captured in crystal structures.

Probing the role of the secondary interface for eIF4A stimulation

To quantify the contributions of the primary and secondary interfaces to the interaction of eIF4A and eIF4G, the isolated N- and C-terminal RecA-domains of eIF4A (RecA_N, RecA_C) were titrated with eIF4G via ITC (Figures 1C and Supplementary Figure 3). The K_d value for the RecA_C/eIF4G complex was $1.3 \pm 0.2\,\mu M$, compared to $0.6 \pm 0.1\,\mu M$ for full-length eIF4A. No binding of RecA_N to eIF4G was detected. From the corresponding free energies of complex dissociation for eIF4A/eIF4G ($\Delta G = 34.3\,kJ/mol$) and RecA_C/eIF4G ($\Delta G = 32.5\,kJ/mol$), a contribution by the secondary interface to complex stability of only ~5% can be calculated ($\Delta\Delta G = \Delta G_{RecA\_N/eIF4G} = -1.8\,kJ/mol$). Our observations are consistent with the different extents of the two interfaces in the crystal structure, and extend and quantify previous data that point toward a (small) contribution of RecA_N to binding (26).

The secondary interface mainly consists of ionic interactions between E43 (eIF4A) and R835 (eIF4G), and a salt bridge between R35 (eIF4A) and D842 (eIF4G) (28) (Figure 1A). In line with a stabilization of the secondary interface by ionic interactions, the eIF4G-imposed conformation of eIF4A was lost with increasing salt concentrations (Supplementary Figure 4). These salt concentrations were lower than the ones required to disrupt the eIF4A/eIF4G complex (26), confirming a critical role of ionic interactions for the secondary interface in general. To probe the role of the secondary interface for the functional interaction of eIF4A and eIF4G, we created mutants that lack the ionic interaction in this interface formed between E43 and R835 (eIF4A_E43R, eIF4G_R835D), or where the side chains have been swapped (eIF4A_E43R and eIF4G_R835E). In addition, an eIF4G mutant containing three negative charges was created (eIF4G_K831E/S834D/R835E; eIF4G_3$^-$). In ITC experiments with eIF4A and eIF4G_R835E and eIF4G_3$^-$, K_d values of $1.0 \pm 0.1\,\mu M$ and $1.1 \pm 0.1\,\mu M$ were obtained. These values are similar to the K_d value of $1.3 \pm 0.2\,\mu M$ for the isolated RecA_C domain, supporting that the mutations in eIF4G_R835E and eIF4G_3$^-$ disrupt the secondary interface (Supplementary Figure 3). Interestingly, eIF4A_E43R titrations with eIF4G yielded a K_d value of $0.2 \pm 0.02\,\mu M$ (Supplementary Figure 3), pointing toward an intact secondary interface and increased overall complex stability. The eIF4G-imposed conformation of eIF4A_E43R was lost at higher salt concentrations than with wild-type eIF4A (Supplementary Figure 4), in line with the secondary interface being stabilized by ionic interactions.

In smFRET experiments, eIF4G_R835E (and eIF4G_R853D, data not shown) only caused a negligible shift in FRET efficiency of eIF4A_Q186/G370C (Figure 3A). With eIF4G_3$^-$, no shift in FRET efficiency was detected. Thus, eIF4G mutants that cannot form the secondary interface fail to impose the eIF4G-specific conformation on eIF4A. In experiments with eIF4A_E43R, eIF4G was still able to induce the same shift in FRET efficiency as with wild-type eIF4A. When eIF4G_R835E was added to eIF4A_E43R, a combination where the ionic interaction should be restored, only a partial shift in E_{FRET} was observed, pointing toward a more complex interaction network in the secondary interface than a binary interaction between E43 and R835. The eIF4G_3$^-$ mutant had lost the ability to affect the eIF4A_E43R conformation. The effect of eIF4G-mutations on the eIF4A conformation is largely paralleled by their effect on the ATPase stimulation (Figure 3B and C). While eIF4G stimulates the wild-type eIF4A ATPase activity 5-fold, eIF4G_R835E and eIF4G_3$^-$ did not stimulate eIF4A, confirming a role of these residues for the functional interaction between eIF4A and eIF4G. In addition, eIF4G was still able to stimulate the ATPase of eIF4A_E43R 3-fold (Figure 3B), in agreement with the ability of this mutant to undergo the eIF4G-induced conformational change (see also 'Discussion' section). The compensatory mutation in eIF4G, R835E, did not restore the 5-fold stimulation as observed in the wild-type context. Instead, this mutant was not able to stimulate eIF4A_E43R, in agreement with its reduced capacity to induce the conformational change (Figure 3A). Similarly, the ATPase stimulation was lost completely with eIF4G_3$^-$.

Overall, our experiments for the first time unambiguously link the global orientation of eIF4A in the complex to the stimulatory effect of eIF4G (Figure 3C), and demonstrate the crucial role of ionic interactions in the secondary interface for imposing the complex-specific conformation on eIF4A.

Downloaded from https://academic.oup.com/nar/article-abstract/39/6/2260/2411439/eIF4G-stimulates-the-activity-of-the-DEAD-box
by WWZ Bibliothek (Oeffentliche Bibliotherk der UniversitÃ¤t Basel) user
on 10 October 2017

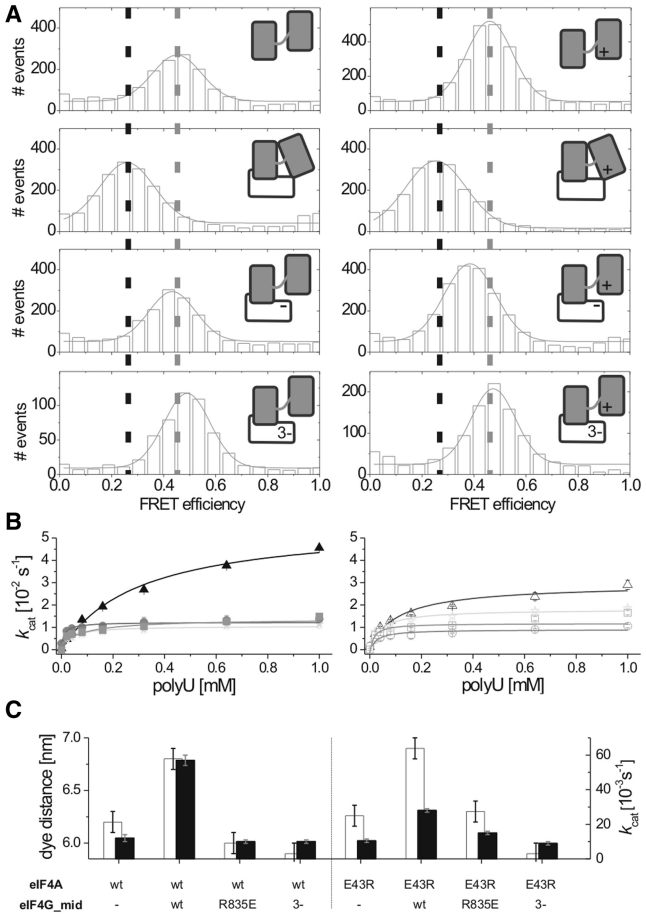

Figure 3. Probing the role of the secondary interface for eIF4G stimulation of eIF4A. (**A**) smFRET histograms for donor/acceptor labeled eIF4A_Q186/G370C (left) and eIF4A_Q186/G370C_E43R (right) in the presence of eIF4G, eIF4G_R835E, and eIF4G_3^{-}. While eIF4G causes a significant shift in FRET efficiency upon binding, this effect is lost with eIF4G_R835E and eIF4G_3^{-}, indicative of a disruption of the secondary interface. For eIF4A_E43R, eIF4G causes a significant shift in FRET efficiency upon binding to eIF4A_E43R. This effect is reduced with eIF4G_R835E and lost with eIF4G_3^{-}. The broken lines indicate the center of the FRET distribution of eIF4A (gray broken lines) and eIF4A/eIF4G (black broken lines). (**B**) Steady-state ATPase activity of eIF4A (left, black squares) and eIF4A_E43R (right, open squares) and stimulation by eIF4G (black and open triangles), eIF4G_R835E (black and open stars), and eIF4G_3^{-} (black and open circles). The k_{cat} values are $k_{cat} = 0.012 \pm 0.002\,s^{-1}$ (eIF4A), $k_{cat} = 0.057 \pm 0.003\,s^{-1}$ (eIF4A/eIF4G), $k_{cat} = 0.010 \pm 0.001\,s^{-1}$ (eIF4A/eIF4G_R835E) and $k_{cat} = 0.010 \pm 0.001\,s^{-1}$ (eIF4A/eIF4G_3^{-}). For eIF4A_E43R, the values are $k_{cat} = 0.011 \pm 0.001\,s^{-1}$; $k_{cat} = 0.028 \pm 0.001\,s^{-1}$ (+eIF4G), $k_{cat} = 0.015 \pm 0.001\,s^{-1}$ (+eIF4G_R835E) and $k_{cat} = 0.009 \pm 0.001\,s^{-1}$ (+eIF4G_3^{-}). (**C**) The ability of eIF4G to induce a conformational change (white bars) is correlated with the extent of stimulation of eIF4A's ATPase activity (black bars). An exception is eIF4A_E43R, which still undergoes a conformational change, but shows a reduced ATPase stimulation. Presumably, the increased eIF4A_E43R/eIF4G complex stability impairs the transition to the catalytically active closed conformation.

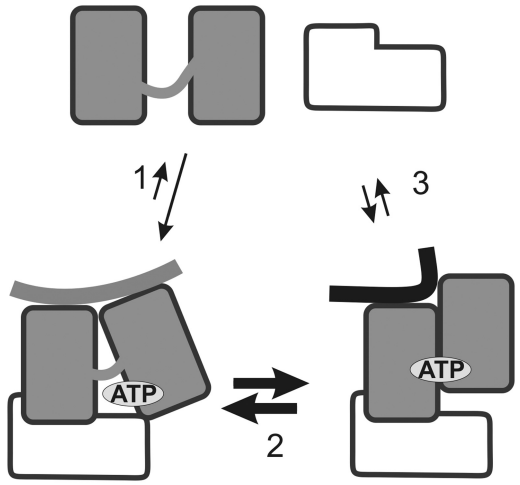

Figure 4. Model for conformational changes of eIF4A and influence of eIF4G. In combination with crystal structures of eIF4A/eIF4G [(28), PDB ID 2vso] and eIF4A(-III) in the closed conformation [(18,19), PDB IDs 2j0s, 2hyi], our FRET data support a model for eIF4G-mediated eIF4A stimulation that is based on three different eIF4A conformations: open (top), closed (bottom right) and 'half-open', bottom left. In the absence of eIF4G, eIF4A alternates between the open and the closed conformations (step 3). In the presence of eIF4G, eIF4A is fixed in the 'half-open' conformation and cycles between this conformation and the closed conformation that is formed upon binding of ATP and RNA (step 2). In the 'half-open' conformation, nucleotide exchange and phosphate release are facilitated. Possibly, the RNA affinity is not reduced to the same extent as in the open conformation, and eIF4A may remain bound to the RNA (gray) in the eIF4G-stimulated catalytic cycle. See main text for details.

Mechanism of the stimulatory effect of eIF4G on eIF4A

With distance restraints derived from experimental FRET efficiencies, we have defined the global conformation of eIF4A in the absence of ligands in solution. Together with structural information (18,19,28), a picture emerges in which eIF4A can switch between three different conformations: open (this work) and closed (18,19), and 'half-open' as imposed by eIF4G [(28), Figure 4]. Careful inspection of the eIF4A structure in complex with eIF4G reveals two salient features (Figure 5): First, the two RecA domains are held apart such that the nucleotide-binding site formed by conserved motifs I and II and the Q-motif in RecA_N is accessible via a channel between the two domains. At the same time, a bound nucleotide cannot establish interactions with both RecA domains as in the closed conformation (Figure 5A and B). In line with an accessible nucleotide binding site in the complex, the affinity of eIF4A for ADP and ATP is moderately decreased in the presence of eIF4G (Supplementary Figure 5). Yet, it is higher than the nucleotide affinity of RecA_N, suggesting some contributions of RecA_C to nucleotide binding that are reduced in complex with eIF4G. Second, even though the two RecA domains are held apart in the region proximal to the eIF4A/eIF4G interface, they are close to each other distal to the interaction site with eIF4G. As a consequence, motifs Ia (PTRELA, RecA_N) and the QxxR-motif (RecA_C) that contribute to the RNA-binding site of eIF4A in the closed conformation are in close proximity. In the crystal, a second eIF4A molecule is close to this region, juxtaposed in an orientation that aligns the same face of the N-terminal RecA domain of one molecule with the C-terminal RecA

Downloaded from https://academic.oup.com/nar/article-abstract/39/6/2260/2411439/eIF4G-stimulates-the-activity-of-the-DEAD-box
by WWZ Bibliothek (Oeffentliche Bibliotherk der UniversitÃ¤t Basel) user
on 10 October 2017

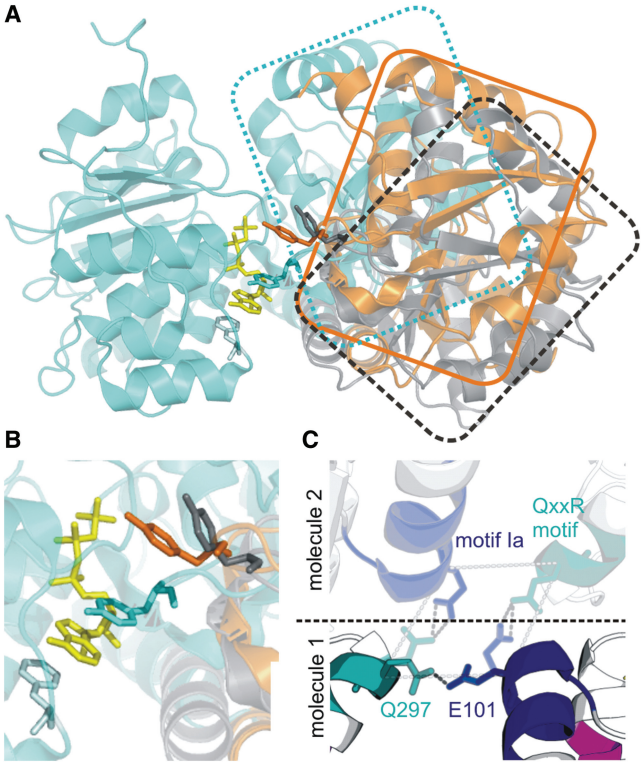

Figure 5. Features of the eIF4A/eIF4G complex. (**A**) Superposition of eIF4A in the reconstructed open (orange), and the closed (cyan, PDB-ID 2hyi) and 'half-open' (gray, PDB-ID 2vso) conformations. The C-terminal RecA domain is represented by the structure of RecA_C in eIF4A-III, in the same orientation as RecA_C of eIF4A in the open and 'half-open' conformations to point out the effect of the different domain orientations on the position of Y371 (stick presentation, F354 in eIF4A). In the closed conformation of eIF4A-III, this residue stacks onto the adenine base. The region around the corresponding F354 in eIF4A has not been resolved in the eIF4A/eIF4G structure. The distance between the nucleotide and the aromatic residue increases from the closed to the open and the 'half-open' conformations. The conserved phenylalanine from the Q-motif that contacts the base (F58, pale blue, F42 in eIF4A) and ADPNP (yellow) are shown in stick representation. As a guide to the eye, the shape of RecA_C is outlined. (**B**) Close-up view of the nucleotide-binding site from A. (**C**) Possible interaction in the 'half-open' conformation between conserved motif Ia (blue) in RecA_N and the QxxR motif (cyan) in RecA_C. In the crystal structure, an intermolecular contact is assigned between E101 to Q297 in a second eIF4A molecule (pale, top), but the corresponding intramolecular interaction (bottom) between E101 to Q297 is conceivable if different side-chain rotamers are populated. See Figure 1A for the location of E101 and Q297.

domain of the second molecule, and vice versa. An interaction between E101 in motif Ia from one molecule with Q297 on motif QxxR from the second molecule has been assigned in the crystal structure. However, the geometry would also be consistent with an intramolecular interaction between E101 and Q297 being formed in this conformation (Figure 5C). Thus, eIF4G may keep the nucleotide-binding pocket accessible, while at the same time maintaining close contact(s) between the two RecA domains.

To test whether the interaction between E101 and Q297 is present in solution and contributes to the stabilization of the eIF4A conformation imposed by eIF4G, we created the eIF4A mutants E101A, Q297A, Q296/297A, Q297R and Q297E. The ATPase activity of eIF4A_Q297A was increased 2.5-fold by eIF4G, compared to 5-fold for wild-type eIF4A (Supplementary Figure 6). However, in smFRET experiments all of these eIF4A mutants adopted a wild-type-like conformation when bound to eIF4G (Supplementary Figure 6). Hence, an interaction between these two motifs from both RecA domains in complex with eIF4G is not the only determinant for stabilizing the 'half-open' conformation, but it may contribute to the observed ATPase stimulation.

How can imposing a 'half-open' conformation result in the stimulation of eIF4A's ATPase activity by eIF4G? An exposed nucleotide-binding pocket predicts rapid nucleotide exchange. We therefore measured nucleotide-binding kinetics in stopped flow experiments using mantADP (Figure 6A and B, and Supplementary Figure 7) under pseudo-first-order conditions. Binding was followed via energy transfer from a tryptophan introduced into eIF4A (Y22W) to the mant group, or from the natural tryptophans in eIF4G to the mant group. Interestingly, transients for nucleotide binding to eIF4A followed double exponential functions both in the absence and in the presence of eIF4G (Figure 6A and B). Both observed rate constants increased with the mantADP concentration, and were increased 2–4-fold in the presence of eIF4G. The data can be described with a general two-step binding model [Figure 6B; (34)]. Two kinetic phases in mant-nucleotide binding might be caused by a transesterification of the mant group between the 2′- and 3′-hydroxyls of the ribose. However, mantADP binding to RecA_N, a control for a completely accessible nucleotide-binding pocket (without any effect from RecA_C), follows single exponential kinetics (Figure 6A and B, see below), arguing against this explanation. In addition, the observed rate constants for nucleotide binding to RecA_N were significantly higher than the rate constants for binding to complete eIF4A (Figure 6A and B, and Supplementary Figure 7), pointing toward an inhibition of nucleotide exchange by RecA_C. Thus, the second slow phase most likely results from contributions of RecA_C to nucleotide binding.

The observed rate constants for mantADP binding to eIF4A did not increase in the presence of eIF4G_R835E (Figures 6B and Supplementary Figure 7), a mutant that still binds to eIF4A via the primary interface, but neither affected the eIF4A conformation nor its ATPase activity. Overall, these results confirm that eIF4G moderately accelerates nucleotide exchange by stabilizing eIF4A in a conformation with an accessible nucleotide-binding pocket. However, the effect of eIF4G is small compared to *bona fide* nucleotide exchange factors.

An efficient stimulation of eIF4A by eIF4G requires an effect on the rate-limiting step of the catalytic cycle. In the nucleotide cycle of the DEAD box protein DbpA, release of phosphate has been identified as the rate-limiting step (36). Therefore, we measured phosphate release from eIF4A in the absence and presence of eIF4G (Figure 6C) and directly compared it to mantADP release under the same conditions. mantADP

Downloaded from https://academic.oup.com/nar/article-abstract/39/6/2260/2411439/eIF4G-stimulates-the-activity-of-the-DEAD-box
by WWZ Bibliothek (Oeffentliche Bibliotherk der UniversitÃ¤t Basel) user
on 10 October 2017

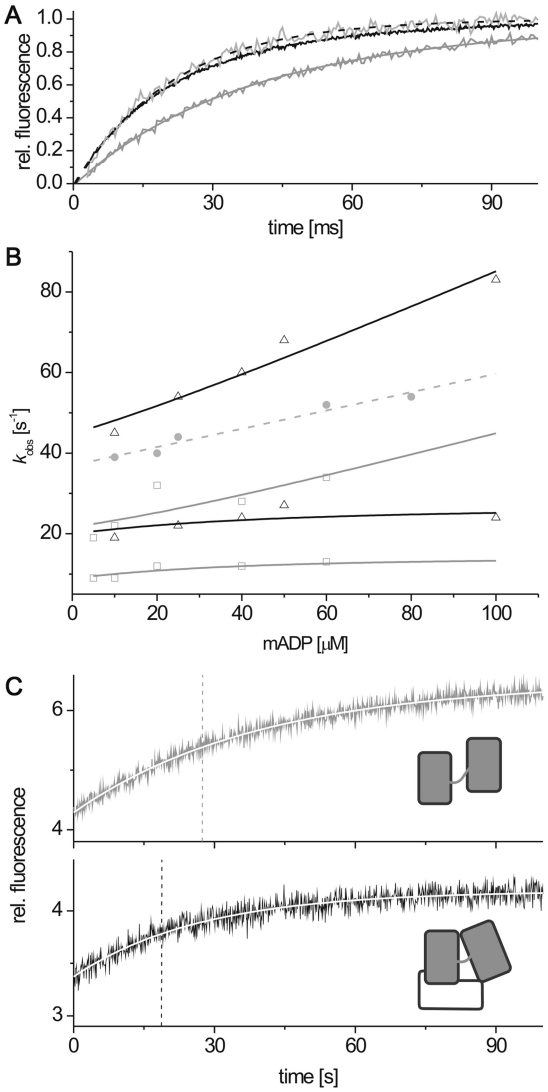

Figure 6. Nucleotide binding and phosphate release kinetics. (**A**) Kinetic transients for 40 μM mantADP binding to RecA_N (black broken lines), eIF4A/eIF4G (black solid line) and eIF4A (gray solid line). Nucleotide binding to eIF4A is accelerated in the presence of eIF4G and occurs with a similar velocity as nucleotide binding to RecA_N. (**B**) Observed rate constants for nucleotide binding to RecA_N (gray circles, gray broken lines), eIF4A/eIF4G (open triangles, black solid line) and eIF4A (open gray squares, gray solid line). Analysis with a general two-step binding model (34) yields the individual rate constants $k_1 = 0.28\,\mu M\,s^{-1}$, $k_{-1} = 15.9\,s^{-1}$, $k_2 = 12.0\,s^{-1}$ and $k_{-2} = 2.5\ s^{-1}$ in the absence, and $k_1 = 0.45\,\mu M\,s^{-1}$, $k_{-1} = 37.2\,s^{-1}$, $k_2 = 23.9\,s^{-1}$ and $k_{-2} = 3.4\,s^{-1}$ in the presence of eIF4G. Nucleotide exchange is accelerated by eIF4G. Nucleotide binding to eIF4A-RecA_N occurs in one step with $k_1 = 0.23\,\mu M\,s^{-1}$ and $k_{-1} = 36.9\,s^{-1}$. The two phases observed for eIF4A and eIF4A/eIF4G point towards contributions of the C-terminal RecA domain. (**C**) Phosphate release from eIF4A (gray) and eIF4A/eIF4G (black). Rate constants are $0.025 \pm 0.001\,s^{-1}$ in the absence and $0.037 \pm 0.001\,s^{-1}$ in the presence of eIF4G. The broken lines indicate the half-times of the reactions.

release from eIF4A occurred with a rate constant of $97 \pm 6\,s^{-1}$ in the absence, and $95 \pm 3\,s^{-1}$ in the presence of polyU-RNA (Supplementary Figure 8). Upon addition of eIF4G, these dissociation rate constants increased to $200 \pm 17\,s^{-1}$ and $169 \pm 8\,s^{-1}$, respectively. Thus, RNA does not affect mantADP release from eIF4A, but eIF4G promotes a 2-fold increase. Phosphate release from eIF4A occurred with a rate constant of $0.025 \pm 0.001\,s^{-1}$ in the presence of RNA, and was accelerated to $0.035 \pm 0.001\,s^{-1}$ in the presence of eIF4G (Figure 6C). These rate constants are several orders of magnitude smaller than those for (mant)ADP release, hence phosphate release is the rate-limiting step in the eIF4A nucleotide cycle in the presence of RNA. The values also show reasonable agreement with the steady-state ATPase rates ($0.012\,s^{-1}$ versus $0.050\ s^{-1}$), confirming that under these conditions, phosphate release is indeed rate limiting. Thus, eIF4G does affect the rate-limiting step in the eIF4A nucleotide cycle and thereby stimulates its ATPase activity. The overall stimulatory effect, however, is small.

DISCUSSION

The conformational states of DEAD box proteins are at the heart of their RNA unwinding activity (3,23,37). Stabilizing the open or the closed conformation of DEAD box proteins thus constitutes a logical way to regulate their activity. For eIF4A, two examples for regulation that target the conformational change have been described: The tumor suppressor protein Pdcd4 inhibits eIF4A activity and, consequently, translation initiation (38) by binding to both domains of eIF4A and preventing the formation of the closed state (39). A similar mechanism may underlie the inhibition of eIF4A by an RNA aptamer that contacts both RecA domains (40). On the other hand, components of the exon-junction complex stabilize eIF4A-III in the closed conformation and prevent re-opening of the inter-domain cleft (18,19). Thereby, ATP hydrolysis still occurs, but product release is inhibited (20), trapping eIF4A-III in the closed conformation with a high affinity for its RNA substrate. A first model for eIF4G action suggested a similar stabilization of the closed state as the basis for eIF4A activation (26). However, cycling between the two conformations is required for DEAD box protein activity. The example of eIF4A-III already illustrates that stabilization of the closed conformer alone does not lead to activation but to inhibition.

Here, we have defined the conformation of eIF4A in solution in the absence of ATP and RNA that is largely different from the crystal structure. In conjunction with previously reported crystal structures of the closed and the eIF4G-stabilized conformations, our results now provide the necessary framework to interpret the mechanism of eIF4A activation by eIF4G. In free eIF4A, the two RecA-domains are separated to a much lesser extent than the previously reported crystal structure suggested. The conserved motifs involved in nucleotide and RNA binding are already oriented toward the inter-domain cleft, whereas they are facing further away from each other in the crystal structure. As a result, the previously suggested stopper function for eIF4A is not required. Instead, by stabilizing the 'half-open' conformation eIF4G acts as a conformational guide toward the closed conformation. The complex between eIF4A and eIF4G is

Downloaded from https://academic.oup.com/nar/article-abstract/39/6/2260/2411439/eIF4G-stimulates-the-activity-of-the-DEAD-box
by WWZ Bibliothek (Oeffentliche Bibliotherk der UniversitÃ¤t Basel) user
on 10 October 2017

stabilized by interactions of eIF4G with the C-terminal RecA domain of eIF4A, the primary interface. In this respect, eIF4G is reminiscent of (covalently attached) extensions to the helicase core that can be found in other DEAD box proteins (3). Our data corroborate that the secondary interface, although not required for overall complex stability, is indispensable for imposing the 'half-open' conformation on eIF4A, and thus essential for the functional interaction between eIF4A and eIF4G.

Due to their negligible energetic contributions to the interface stability, the critical residues in the secondary interface that are responsible for aligning eIF4A in the 'half-open' conformation are difficult to pinpoint. The salt bridge between R35 (eIF4A) and D842 (eIF4G) has been probed previously (28), and no consistent results were obtained. eIF4G_D842R was still able to form a complex with eIF4A and to stimulate ATPase activity. By contrast, no complex formation was observed with eIF4A_R35D, even though the interaction through the primary interface was unperturbed. Surprisingly, both mutants were capable of stimulating eIF4A's ATPase activity to similar extents as wild type. In our hands, the R35D mutation in eIF4A disrupts the secondary interface (Supplementary Figure S4). We have probed the second ionic interaction between E43 (eIF4A) and R835 (eIF4G), and find that R835 in eIF4G is required for imposing the 'half-open' conformation on eIF4A and for stimulation of its ATPase activity, whereas E43 in eIF4A is not. Our data argue against binary interactions between these ionic side chains in the secondary interface, but are consistent with a network of ionic interactions that allows for flexibility. Similarly, a dynamic network of multiple weak, but specific interactions has already been proposed for the functional interaction between human eIF4A, eIF4G and eIF4H (27). The regulation of eIF4A by eIF4G may thus be in stark contrast to the clamp-like regulation of eIF4A-III.

Mechanism of eIF4A activation and implications for its regulation in translation

It has previously been suggested that eIF4G acts as a 'stopper' that prevents the N-terminal RecA domain from moving away too far (28). However, we have shown that the RecA domains are already considerably close to each other in the open conformation, hence such a stopper function is not required. More importantly, the eIF4A/eIF4G complex forms a channel that in principle allows the access to and exit from the nucleotide-binding pocket of eIF4A. We have demonstrated here that in this conformation, nucleotide release and phosphate release are accelerated. Phosphate release (or an associated conformational change) is the rate-limiting step in the DEAD box protein catalytic cycle (36), rendering it a key step for efficient regulation. The tight interaction between eIF4A and eIF4G via the primary interface provides an anchor, such that a stable complex will be maintained even if the secondary interface is disrupted. Thus, the two interfaces in conjunction allow for eIF4A to switch into the closed conformation upon ATP and RNA binding, while maintaining a stable interaction with eIF4G. In this model, the N-terminal RecA domain will alternate between interactions with eIF4G in the 'half-open' conformation and the C-terminal domain of eIF4A in the closed conformation. As phosphate release and nucleotide exchange appear to be possible in the eIF4G-bound conformation, no complete opening is required for product release. If eIF4A does not completely re-open, the RNA affinity may not be reduced to the same extent as in the open conformation. Possibly, RNA is not released, providing an explanation for the increase in eIF4A processivity upon interaction with eIF4G and H (6,27).

The importance of eIF4A dynamics within the eIF4A/eIF4G complex and its link to the weak interactions in the secondary interface becomes evident from the effect of the E43R mutation. This mutation leads to a stabilization of the secondary interface, but at the same time eIF4A_E43R is stimulated less efficiently by eIF4G (2.5-fold versus 5-fold for wild-type eIF4A). Presumably, this mutant of eIF4A is fixed in the eIF4G-type conformation, and hindered from efficiently proceeding through the catalytic cycle. The destabilizing effect of E43 on the secondary interface thus underlines the requirement for weak interactions that can easily be overcome for activating eIF4A. A variety of regulation mechanisms that affect the conformational change can be envisaged. Presumably, more stimulatory proteins that regulate DEAD box protein activity by accelerating this step will be identified in the future.

Altogether, eIF4G thus plays a more active role in regulating eIF4A activity than proposed in previous models. Its regulatory effect, however, is subtle. During the initiation of eukaryotic translation, a large number of translation factors act in a concerted fashion, and synergistic effects may allow for the amplification of eIF4G's subtle effect by other translation initiation factors. In this picture, eIF4A would amplify and integrate all of these input signals and thus act as a regulatory hub in translation initiation.

SUPPLEMENTARY DATA

Supplementary Data are available at NAR Online.

ACKNOWLEDGEMENTS

We thank Ulrich Baumann (University of Bern/University of Cologne) for kindly providing the expression constructs for yeast eIF4A and the eIF4G middle domain, Caroline Loew for help with ITC experiments, and Ines Hertel for excellent technical support.

FUNDING

VolkswagenStiftung (to D.K.); Swiss National Science Foundation (to D.K.); Roche Research Foundation (to M.H.). The open access publication charge for this paper has been waived by Oxford University Press—*NAR* Editorial Board members are entitled to one free paper

Downloaded from https://academic.oup.com/nar/article-abstract/39/6/2260/2411439/eIF4G-stimulates-the-activity-of-the-DEAD-box
by WWZ Bibliothek (Oeffentliche Bibliotherk der UniversitÃ¤t Basel) user
on 10 October 2017

per year in recognition of their work on behalf of the journal.

Conflict of interest statement. None declared.

REFERENCES

1. Kapp,L.D. and Lorsch,J.R. (2004) The molecular mechanics of eukaryotic translation. *Annu. Rev. Biochem.*, **73**, 657–704.
2. Jackson,R.J., Hellen,C.U. and Pestova,T.V. (2010) The mechanism of eukaryotic translation initiation and principles of its regulation. *Nat. Rev. Mol. Cell Biol.*, **11**, 113–127.
3. Hilbert,M., Karow,A.R. and Klostermeier,D. (2009) The mechanism of ATP-dependent RNA unwinding by DEAD box proteins. *Biol. Chem.*, **390**, 1237–1250.
4. Rogers,G.W. Jr, Richter,N.J. and Merrick,W.C. (1999) Biochemical and kinetic characterization of the RNA helicase activity of eukaryotic initiation factor 4A. *J. Biol. Chem.*, **274**, 12236–12244.
5. Rogers,G.W. Jr, Komar,A.A. and Merrick,W.C. (2002) eIF4A: the godfather of the DEAD box helicases. *Prog. Nucleic Acid Res. Mol. Biol.*, **72**, 307–331.
6. Rogers,G.W. Jr, Richter,N.J., Lima,W.F. and Merrick,W.C. (2001) Modulation of the helicase activity of eIF4A by eIF4B, eIF4H, and eIF4F. *J. Biol. Chem.*, **276**, 30914–30922.
7. Korneeva,N.L., First,E.A., Benoit,C.A. and Rhoads,R.E. (2005) Interaction between the NH2-terminal domain of eIF4A and the central domain of eIF4G modulates RNA-stimulated ATPase activity. *J. Biol. Chem.*, **280**, 1872–1881.
8. Rozovsky,N., Butterworth,A.C. and Moore,M.J. (2008) Interactions between eIF4AI and its accessory factors eIF4B and eIF4H. *RNA*, **14**, 2136–2148.
9. Svitkin,Y.V., Pause,A., Haghighat,A., Pyronnet,S., Witherell,G., Belsham,G.J. and Sonenberg,N. (2001) The requirement for eukaryotic initiation factor 4A (eIF4A) in translation is in direct proportion to the degree of mRNA 5' secondary structure. *RNA*, **7**, 382–394.
10. Lorsch,J.R. and Herschlag,D. (1998) The DEAD box protein eIF4A. 1. A minimal kinetic and thermodynamic framework reveals coupled binding of RNA and nucleotide. *Biochemistry*, **37**, 2180–2193.
11. Lorsch,J.R. and Herschlag,D. (1998) The DEAD box protein eIF4A. 2. A cycle of nucleotide and RNA-dependent conformational changes. *Biochemistry*, **37**, 2194–2206.
12. Pause,A. and Sonenberg,N. (1992) Mutational analysis of a DEAD box RNA helicase: the mammalian translation initiation factor eIF-4A. *EMBO J.*, **11**, 2643–2654.
13. Pause,A., Methot,N. and Sonenberg,N. (1993) The HRIGRXXR region of the DEAD box RNA helicase eukaryotic translation initiation factor 4A is required for RNA binding and ATP hydrolysis. *Mol. Cell. Biol.*, **13**, 6789–6798.
14. Johnson,E.R. and McKay,D.B. (1999) Crystallographic structure of the amino terminal domain of yeast initiation factor 4A, a representative DEAD-box RNA helicase. *RNA*, **5**, 1526–1534.
15. Benz,J., Trachsel,H. and Baumann,U. (1999) Crystal structure of the ATPase domain of translation initiation factor 4A from *Saccharomyces cerevisiae* – the prototype of the DEAD box protein family. *Structure*, **7**, 671–679.
16. Caruthers,J.M., Johnson,E.R. and McKay,D.B. (2000) Crystal structure of yeast initiation factor 4A, a DEAD-box RNA helicase. *Proc. Natl Acad. Sci. USA*, **97**, 13080–13085.
17. Sengoku,T., Nureki,O., Nakamura,A., Kobayashi,S. and Yokoyama,S. (2006) Structural basis for RNA unwinding by the DEAD-box protein Drosophila Vasa. *Cell*, **125**, 287–300.
18. Andersen,C.B., Ballut,L., Johansen,J.S., Chamieh,H., Nielsen,K.H., Oliveira,C.L., Pedersen,J.S., Seraphin,B., Le Hir,H. and Andersen,G.R. (2006) Structure of the exon junction core complex with a trapped DEAD-box ATPase bound to RNA. *Science*, **313**, 1968–1972.
19. Bono,F., Ebert,J., Lorentzen,E. and Conti,E. (2006) The crystal structure of the exon junction complex reveals how it maintains a stable grip on mRNA. *Cell*, **126**, 713–725.
20. Nielsen,K.H., Chamieh,H., Andersen,C.B., Fredslund,F., Hamborg,K., Le Hir,H. and Andersen,G.R. (2008) Mechanism of ATP turnover inhibition in the EJC. *RNA*, **15**, 67–75.
21. Collins,R., Karlberg,T., Lehtio,L., Schutz,P., van den Berg,S., Dahlgren,L.G., Hammarstrom,M., Weigelt,J. and Schuler,H. (2009) The DExD/H-box RNA helicase DDX19 is regulated by an alpha-helical switch. *J. Biol. Chem.*, **284**, 10296–10300.
22. von Moeller,H., Basquin,C. and Conti,E. (2009) The mRNA export protein DBP5 binds RNA and the cytoplasmic nucleoporin NUP214 in a mutually exclusive manner. *Nat. Struct. Mol. Biol.*, **16**, 247–254.
23. Theissen,B., Karow,A.R., Kohler,J., Gubaev,A. and Klostermeier,D. (2008) Cooperative binding of ATP and RNA induces a closed conformation in a DEAD box RNA helicase. *Proc. Natl Acad. Sci. USA*, **105**, 548–553.
24. Aregger,R. and Klostermeier,D. (2009) The DEAD-box helicase YxiN maintains a closed conformation during ATP hydrolysis. *Biochemistry*, **48**, 10679–10681.
25. Liu,F., Putnam,A. and Jankowsky,E. (2008) ATP hydrolysis is required for DEAD-box protein recycling but not for duplex unwinding. *Proc. Natl Acad. Sci. USA*, **51**, 20209–20214.
26. Oberer,M., Marintchev,A. and Wagner,G. (2005) Structural basis for the enhancement of eIF4A helicase activity by eIF4G. *Genes Dev.*, **19**, 2212–2223.
27. Marintchev,A., Edmonds,K.A., Marintcheva,B., Hendrickson,E., Oberer,M., Suzuki,C., Herdy,B., Sonenberg,N. and Wagner,G. (2009) Topology and regulation of the human eIF4A/4G/4H helicase complex in translation initiation. *Cell*, **136**, 447–460.
28. Schütz,P., Bumann,M., Oberholzer,A.E., Bieniossek,C., Trachsel,H., Altmann,M. and Baumann,U. (2008) Crystal structure of the yeast eIF4A-eIF4G complex: An RNA-helicase controlled by protein–protein interactions. *Proc. Natl Acad. Sci. USA*, **105**, 9564–9569.
29. Studier,F.W. (2005) Protein production by auto-induction in high density shaking cultures. *Protein Expr. Purif.*, **41**, 207–234.
30. Gasteiger,E., Hoogland,C., Gattiker,A., Duvaud,S., Wilkins,M.R., Appel,R.D. and Bairoch,A. (2005) Protein identification and analysis tools on the ExPASy Server. In Walker,J.M. (ed.), *The Proteomics Protocols Handbook*. Humana Press, pp. 571–607.
31. Hiratsuka,T. (1983) New ribose-modified fluorescent analogs of adenine and guanine nucleotides available as substrates for various enzymes. *Biochim. Biophys. Acta*, **742**, 496–508.
32. Adam,H. (1962) *Methoden der enzymatischen Analyse*. Bergmeyer, H.U. (Hrsg.), Verlag Chemie, Weinheim, pp. 573–577.
33. Brune,M., Hunter,J.L., Corrie,J.E. and Webb,M.R. (1994) Direct, real-time measurement of rapid inorganic phosphate release using a novel fluorescent probe and its application to actomyosin subfragment 1 ATPase. *Biochemistry*, **33**, 8262–8271.
34. Johnson,K.A. (1986) Rapid kinetic analysis of mechanochemical adenosinetriphosphatases. *Methods Enzymol.*, **134**, 677–705.
35. Gubaev,A., Hilbert,M. and Klostermeier,D. (2009) The DNA gate of *Bacillus subtilis* gyrase is predominantly in the closed conformation during the DNA supercoiling reaction. *Proc. Natl Acad. Sci. USA*, **106**, 13278–13283.
36. Henn,A., Cao,W., Hackney,D.D. and De La Cruz,E.M. (2008) The ATPase cycle mechanism of the DEAD-box RNA helicase, DbpA. *J. Mol. Biol.*, **377**, 193–205.
37. Karow,A.R. and Klostermeier,D. (2009) A conformational change in the helicase core is necessary but not sufficient for RNA unwinding by the DEAD box helicase YxiN. *Nucleic Acids Res.*, **37**, 4464–4471.
38. Yang,H.S., Jansen,A.P., Komar,A.A., Zheng,X., Merrick,W.C., Costes,S., Lockett,S.J., Sonenberg,N. and Colburn,N.H. (2003) The transformation suppressor Pdcd4 is a novel eukaryotic translation initiation factor 4A binding protein that inhibits translation. *Mol. Cell. Biol.*, **23**, 26–37.
39. Chang,J.H., Cho,Y.H., Sohn,S.Y., Choi,J.M., Kim,A., Kim,Y.C., Jang,S.K. and Cho,Y. (2009) Crystal structure of the eIF4A-PDCD4 complex. *Proc. Natl Acad. Sci. USA*, **106**, 3148–3153.
40. Oguro,A., Ohtsu,T., Svitkin,Y.V., Sonenberg,N. and Nakamura,Y. (2003) RNA aptamers to initiation factor 4A helicase hinder cap-dependent translation by blocking ATP hydrolysis. *RNA*, **9**, 394–407.

Downloaded from https://academic.oup.com/nar/article-abstract/39/6/2260/2411439/eIF4G-stimulates-the-activity-of-the-DEAD-box
by WWZ Bibliothek (Oeffentliche Bibliotherk der UniversitÃ¤t Basel) user
on 10 October 2017